# Sharp notch roots subject to in-plane and anti-plane loading: An alterative normalisation of the eigenfields & their application to example problems

R. Ramesh and D.A. Hills
Department of Engineering Science
University of Oxford
Parks Road, Oxford
OX1 3PJ, UK

**Abstract**

The state of stress at a sharp notch is characterised by the classical Williams eigenfuction expansion for in-plane loading, and a corresponding anti-plane solution. Excluding the case when the internal notch angle is $2\pi$ (a crack), the solutions have differing orders of singularity, and hence, between any pair of modes of loading, there is an internal implied length scale. Here we bring out those length scales, and show how the three generalised stress intensity factors may be replaced by equivalent parameters having a much more direct physical interpretation. The revised form of the semi-infinite notch solutions are then applied to example geometries, showing how the characteristics of the notch-root process zone may be inferred without further calculation.

## 1 Introduction

Figure 1.1 shows a semi-infinite notch of included angle $2\alpha$, with an attached cylindrical coordinate set $r, \theta, z$. If we represent the state of stress in its neighbourhood using an appropriate series representation, and require the faces to be traction-free, the well-known classical Williams solution, together with the corresponding anti-plane solution emerge [1]. The former has been built upon by many others (eg [2, 3, 4, 5]). Research into singularities in boundary value problems has been explored by Grisvard and Leguillon [6, 7] with others looking at non-smooth domains [8, 9]. It has been used extensively for estimating the plastic process zones [10, 11, 12, 13, 14, 15] of notches and cracks. A great deal of work has also been done on evaluating stress intensity factors in increasingly complex geometries [16]. Stress intensity factors are particularly useful when determining the fatigue limit [17, 18]. Some anal-

ysis has also been carried out to determine a suitable criterion for crack nucleation [19, 20] since the fatigue life of many components will be determined by crack nucleation (usually occurs near stress raisers) and propagation. An area of special interest that has been probed is that of rounding [21], since no real notch can be perfectly sharp. There have been many extensions, for example looking at bonded elastically dissimilar wedges [22, 23], and the effect of elastic anisotropy [24, 25, 26, 27, 28]. The starting point of our development of the solution is the following equation:

$$\sigma_{ij}(r,\theta,z) = K_I r^{\lambda_I - 1} f_{ij}^{I}(r,\theta,z) + K_{II} r^{\lambda_{II} - 1} f_{ij}^{II}(r,\theta,z) + K_{III} r^{\lambda_{III} - 1} f_{ij}^{III}(r,\theta,z) \qquad (1.1)$$

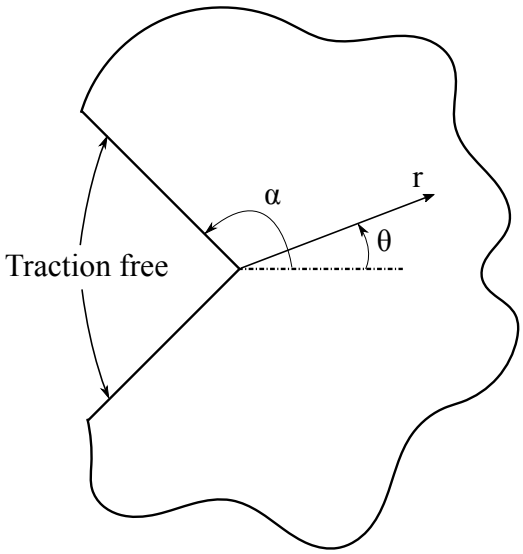



Figure 1.1: Semi-infinite wedge

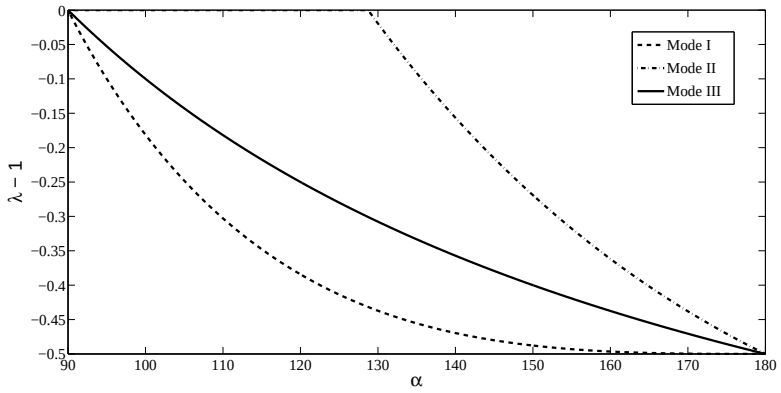



Figure 1.2: Williams solution eigenvalues

where the eigenvalues $\lambda_I, \lambda_{II}, \lambda_{III}$, are known functions of $\alpha$ (see Figure 1.2), the eigenfunctions $f_{ij}^{k}$ (given in the Appendix) are also established, and it will be noted that, if we exclude the solution $2\alpha{=}2\pi$ (a crack), $\lambda_I < \lambda_{II} < \lambda_{III}$. It follows that, as there will always be some plasticity present at the notch root, if the loading is light enough and the material strong enough, we can always establish

a regime under which the process zone is mode $I$ in character. The question which arises is, under combined modes loading, under what conditions is the plasticity zone strongly mode $I$ in character, and when is it either mixed mode or strongly dominated by one of the other eigensolutions? In the past this calculation has not usually been done within the asymptotic form: doing so is an attractive procedure as the results found are universal in nature, in that they may be pasted into any finite problem and the results for mixity employed without further work. We have already done this for the case of a notch subject only to in-plane loading [29, 30], and the object in the present paper is to extend this solution to the case where mode $III$ (anti-plane) loading is present, together with at least one of the two in-plane forms of excitation. To form a consistent notation, we will add superscripts in Arabic numerals to the variables $d_0$, $G_0$. So, starting with a re-iteration of the in-plane loading solution already published, we see that Equation 1.1 may be re-written in the form

$$\frac{\sigma_{ij}(r,\theta)}{G_0^{12}} = \left(\frac{r}{d_0^{12}}\right)^{\lambda_I - 1} f_{ij}^{I}(\theta) + \left(\frac{r}{d_0^{12}}\right)^{\lambda_{II} - 1} f_{ij}^{II}(\theta), \tag{1.2}$$

where

$$d_0^{12} = \left|\frac{K_{II}}{K_I}\right|^{\frac{1}{\lambda_I - \lambda_{II}}} \tag{1.3}$$

$$G_0^{12} = |K_I|^{\frac{\lambda_{II}-1}{\lambda_{II}-\lambda_I}} \, |K_{II}|^{\frac{\lambda_I - 1}{\lambda_I - \lambda_{II}}} \, . \tag{1.4}$$

It is apparent that, in very general terms, the distance $d_0^{12}$ represents the characteristic length scale separating mode $I$ dominated behaviour ($r << d_0^{12}$) and mode $II$ dominated behaviour ($r >> d_0^{12}$). A quantitative way of expressing closeness to either kind of asymptotic form was started in [29] and developed by Flicek and Hills [30].

We first consider the semi-infinite wedge to deduce general properties of the geometry. The solutions may then be pasted into finite problems to show that these observations can be used in a practical problem.

Very close to the notch tip the semi-infinite sharp notch solution dominates the stress field [31]. Thus even though all practical notches will posses a finite radius, the statements made here remain valid at distances large compared to the notch radius and small compared to the nearest feature. Another point to consider is the sensitivity to the sign on the stress intensity factors. This of course practically only applies to $K_I$ the first mode of loading. It has been shown by Churchman et. al. [32] that the closure caused by a negative mode one stress intensity factor does not alter the geometry of the problem greatly.

An implicit assumption that has been made is that only the singular terms have been considered in

the Williams solution. This is because the stress very close the the notch root is dominated by this term. It can be seen in the work by Ayatollahi [33] that the second term does have an effect on the solution however; since we are looking at distances of $r/a < 0.01$ (where $a$ is the distance to the nearest feature) it can be seen that the approximation is a very good one.

## 2 Extension of formulation to mode $III$ behaviour

By analogy with the definitions of the new parameters $G_0^{12}$, expressing the magnitude of loading, and $d_0^{12}$, giving the internal length scale, developed above we may propose new forms giving equivalent information when Mode $III$ loading is present but mode $II$ is absent. Thus the appropriate definitions for alternative notch parameters loaded in mode $I$ and $III$ are:

$$d_0^{13} = \left| \frac{K_{III}}{K_I} \right|^{\frac{1}{\lambda_I - \lambda_{III}}}, \tag{2.1}$$

$$G_0^{13} = |K_I|^{\frac{\lambda_{III}-1}{\lambda_{III}-\lambda_I}} \, |K_{III}|^{\frac{\lambda_I - 1}{\lambda_I - \lambda_{III}}} . \tag{2.2}$$

If mode $I$ loading is absent but mode $II$ is present, the definitions for mode $II$ and $III$ loading are:

$$d_0^{23} = \left| \frac{K_{III}}{K_{II}} \right|^{\frac{1}{\lambda_{II} - \lambda_{III}}}, \tag{2.3}$$

$$G_0^{23} = |K_{II}|^{\frac{\lambda_{III}-1}{\lambda_{III}-\lambda_{II}}} \, |K_{III}|^{\frac{\lambda_{II} - 1}{\lambda_{II} - \lambda_{III}}} . \tag{2.4}$$

By eliminating the stress intensity factors from the $d_0^{ij}$ definitions we can find a relationship between these characteristic lengths, which is

$$(d_0^{23})^{\lambda_{II}-\lambda_{III}} = \frac{(d_0^{13})^{\lambda_I - \lambda_{III}}}{(d_0^{12})^{\lambda_I - \lambda_{II}}}. \tag{2.5}$$

The relationship means that the three variables are not independent. If we choose two of the $d_0$ values, the third is fixed. A number of interesting points can be found from this relationship:

1. $d_0^{12}$ always lies between $d_0^{13}$ and $d_0^{23}$. Thus, all loading regimens can be classified into one of the cases $d_0^{13} < d_0^{23}$ or $d_0^{23} < d_0^{13}$.

2. For the case $d_0^{13} < d_0^{23}$ it is possible to have mode $III$ dominance for distances that lie between $d_0^{13}$ and $d_0^{23}$. When $d_0^{23} < d_0^{13}$ mode $III$ dominance is not possible.

3. If two of the $d_0$ values are equal then the third must also equal this value.

4. For both categories (note 1), very close to the notch root there is certainly mode $I$ dominance. This is because it is the most singular of the three modes.

5. For both categories (note 1), distant from the notch root there is certainly mode $II$ dominance. This is because it is the slowest decaying (least singular) of the three modes.

Looking at the definition of $d_0^{13}$ we can say when $r < d_0^{13}$ mode $I$ is stronger relative to mode $III$ and the converse is true for $r > d_0^{13}$. Figures 2.1 and 2.2 show how single mode dominance can be deduced from these properties.

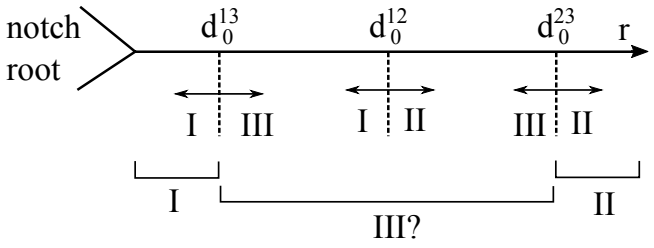



Figure 2.1: Regions of single mode dominance: $d_0^{13} < d_0^{23}$

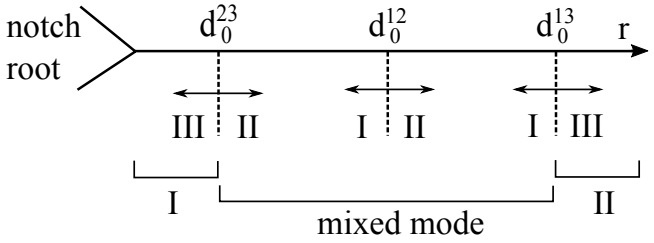



Figure 2.2: Regions of single mode dominance: $d_0^{23} < d_0^{13}$

## 3 Characterisation of plasticity zone

The dominance of a single mode can be found by looking at the shape of the plastic zone. This can be obtained by considering countours of the Von Mises yield criterion for extended elastic behaviour at the notch root. The shape of these fronts can be compared to the solution for the separately excited individual modes of loading and we can determine which mode the loading is closer to. The yield condition is given by

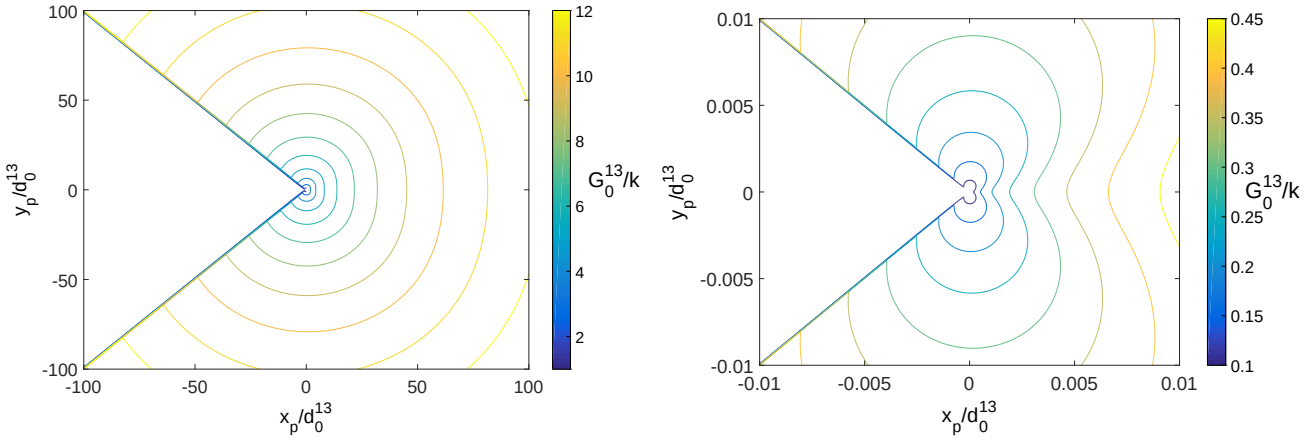
$$3k^2 = J_2 = \frac{1}{3}(\sigma_{11} + \sigma_{22} + \sigma_{33})^2 - \sigma_{11}\sigma_{22} - \sigma_{22}\sigma_{33} - \sigma_{11}\sigma_{33} + \sigma_{12}^2 + \sigma_{13}^2 + \sigma_{23}^2 \tag{3.1}$$

Where $J_2$ is the second deviatoric invariant, and $k$ is the yield stress in pure shear.

### 3.1 Mode $I$ and $III$ loading

In many ways it is easier to carry out an analysis of the proximity of the solution to mode $III$ than it is to either mode $I$ or mode $II$, simply because the implied shape of the plasticity zone under anti-plane loading is a circle. In much of what follows we will consider $2\alpha = 3\pi/2$ to provide illustrative results. With this notch angle $\lambda_I = 0.544484$ and $\lambda_{III} = 0.666667$ so that, at light loads the solution shows mode $I$ dominance and at high loads it shows mode $III$ dominance. The solution studied assumes tranverse plane strain, with a Poisson's ratio of 0.3.

Figure 3.1 are plots which show two extreme cases of the plastic radius where there is dominance of mode $III$ (Figure 3.1a) and mode $I$ (Figure 3.1b) respectively. It can be seen that high values of $G_0^{13}$ give rise to dominance by mode $III$ and low values give mode $I$ dominance. This is illustrated more explicitly in Figure 3.2, where we display the ratio of the plastic radius along $\theta = 0$ to that along $\theta = \pi/2$.




(a) Mode $III$ dominance

(b) Mode $I$ dominance

Figure 3.1: Plastic radius of mixed mode loading

For the case of pure mode $III$ loading $r_p(0) = r_p(\pi/2)$ whereas for mode $I$ loading $r_p(0) = 0.1708 r_p(\pi/2)$. Thus, the ratio $r_p(0)/r_p(\pi/2)$ would seem to be a good, simple measure or closeness of the notch root plastic zone to either the mode $I$ or mode $III$ solution.

We can get a better picture of mode dominance by looking at the whole field rather than just at $\theta = 0$ & $\pi/2$. The general trend as we have noted before shows that high values of $G_0^{13}/k$ yield mode $III$ dominance and low values yield mode $I$ dominance. The percentage error is found by looking at the sum of all the squares of the error between the plastic radius of the mixed mode compared to the pure mode normalised by the pure mode ($k = I, III$).

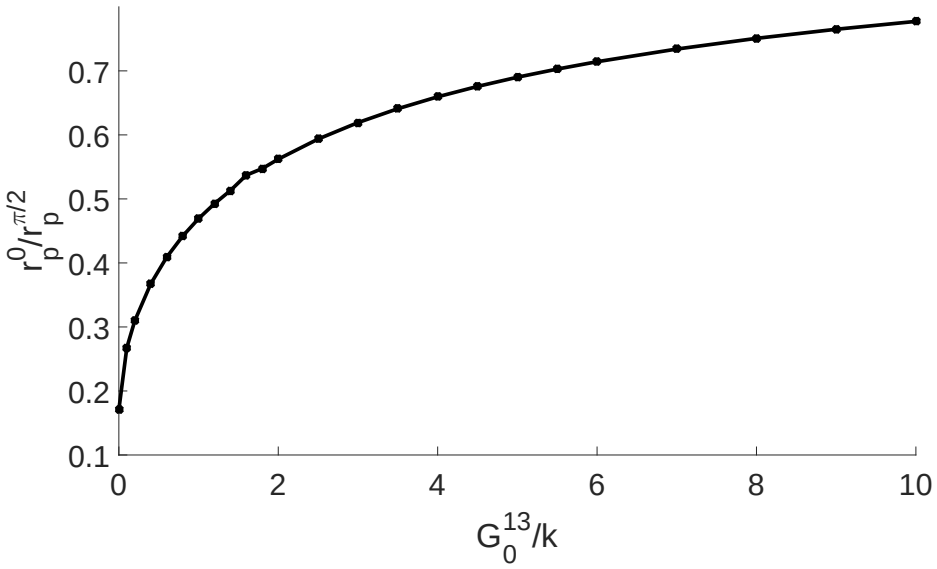
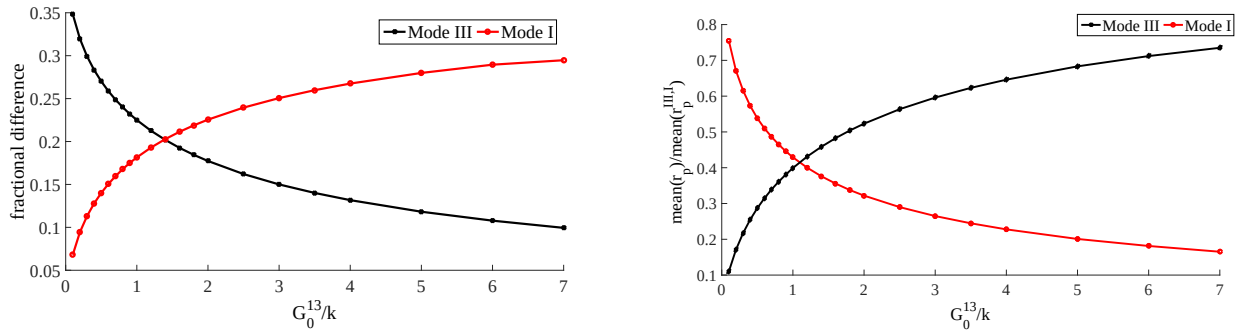



Figure 3.2: Mode $I$ and $III$

$$fractional \quad difference = \frac{\int (r_p^{mm}(\theta) - r_p^k(\theta))^2 d\theta}{\int r_p^k(\theta)^2 d\theta} \tag{3.2}$$

The difference is magnitude is quantified by the mean value of the mixed mode solution normalised by the mean value of the pure mode solution. Figure 3.3 quantifies how close the mixed mode loading is to pure modes of loading ($I$,$III$).




(a) Comparison of the **shape** of mixed loading to pure mode loading

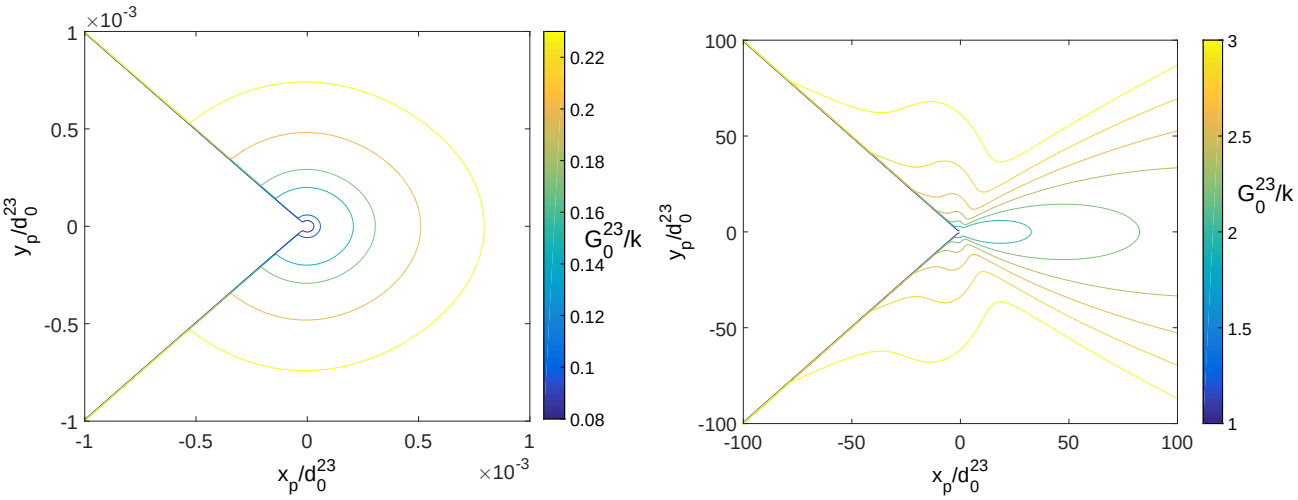
(b) Comparison of the **size** of mixed loading to pure mode loading

Figure 3.3: Comparison of mode dominance

## 3.2 Mode $II$ and $III$ loading

We now look at what happens when only modes $II$ and $III$ loading are present and again we treat extensively the case $2\alpha = 3\pi/2$. The value of $\lambda_{II} = 0.90853$ so that light loads now give rise to a mode $III$ characteristic solution and heavy loads have a mode $II$ characteristic. Figure 3.4 shows the implied plastic zone sizes and shapes at light and heavy loads. Again we realise that the ratio

$r_p(\pi/2)/r_p(0)$ provides a good measure of the similarity between the plastic zone shape and those under pure mode $III$ loading (where, as before, this ratio is unity) and under pure mode $II$ loading, where the ratio goes to zero. The results of these calculations are summarised in Figure 3.5.




(a) Mode $III$ dominance (b) Mode $II$ dominance

Figure 3.4: Plastic radius of mixed mode loading

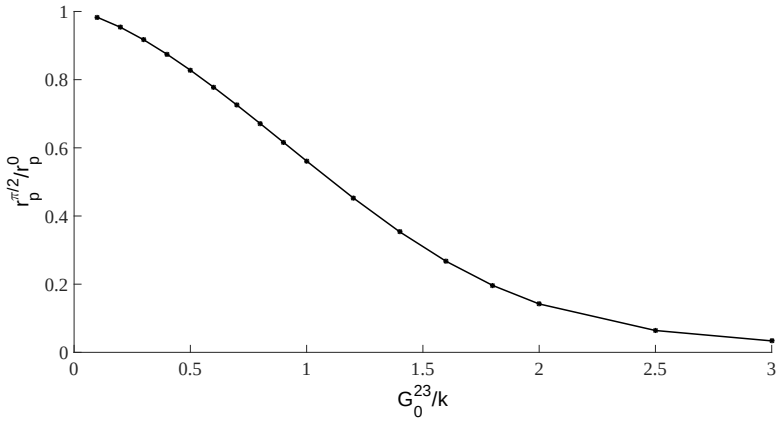
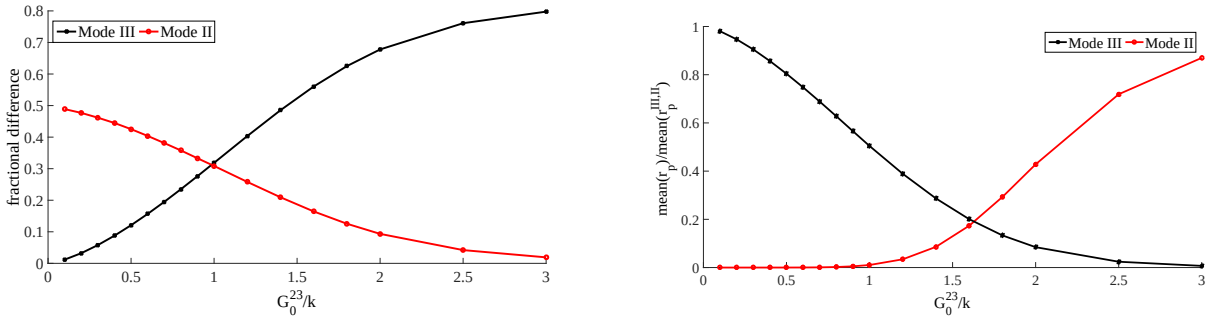



Figure 3.5: Mode $II$ and $III$




(a) Comparison of the **shape** of mixed loading to pure mode loading (b) Comparison of the **size** of mixed loading to pure mode loading

Figure 3.6: Comparison of mode dominance

Looking at the whole field we can better quantify the mode dominance by looking at the overall shape rather than just along $\theta = 0$ & $\pi/2$. Figure 3.6 agrees with what we found looking at just $r_p(0)$ and $r_p(\pi/2)$, low $G_0^{23}/k$ gives rise to mode $III$ dominance and mode $II$ under under large values of $G_0^{23}/k$.

# 4 Finite Example Problems

We now apply the solutions we have derived to a consideration of some simple example finite problems, and examine how they enable us to characterise how like the fundamental separate modes of loading the implied plasticity (and hence process zones) are. First, we note definitions of the stress intensity factors and their separation along the notch bisector. We define the calibrations of the different modes

$$K_k = \Lambda_k \sigma_0 a^{1-\lambda_k} \tag{4.1}$$

where the stress along the bisector such that $\theta = 0$ allows us to write the following:

$$\sigma_{ij}(r,0) = K_k r^{\lambda_i - 1} f_{ij}^k(0) \qquad k = I, II, III \tag{4.2}$$

where $a$ is the characteristic distance to the nearest feature and $\sigma_0$ is the reference stress. We have defined the eigenvectors in such a way that they are unity when $\theta = 0$ ($f_{ij}^k(0) = 1$) thus we can use equation 4.2 to get $K_i$ and substitute it into Equation 4.1 to get $\Lambda_i$.

## 4.1 Notched cylinder under tension and torsion (Mode $I$ and $III$)

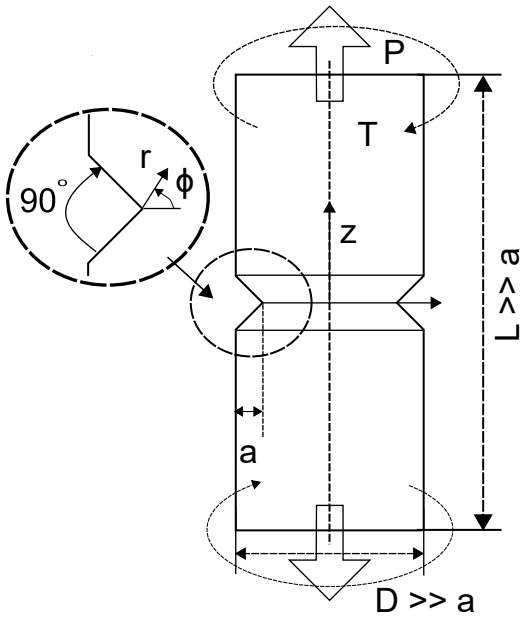



Figure 4.1: Mode $I$ and $III$

$$\begin{Bmatrix} K_I a^{\lambda_I - 1} \\ K_{III} a^{\lambda_{III} - 1} \end{Bmatrix} = \begin{bmatrix} 0.97786 & 0 \\ 0 & 1.0873 \end{bmatrix} \begin{Bmatrix} \sigma_0 \\ \tau_T \end{Bmatrix} \tag{4.3}$$

Where $\sigma_0$ is the remote stress due to the axial load, $P$, away from the notch and $\tau_T$is the shear stress induced by a torque, $T$, at the outer radius, $a$, of the rod away from the notch. Let

$$\sigma_0 = \frac{4P}{\pi D^2}, \tag{4.4}$$

$$\tau_T = 16TD^3. \tag{4.5}$$

Use the definition of $d_0^{13}$ to give

$$\frac{r}{a} = \frac{r}{d_0^{13}} \frac{1}{a} \left| \frac{K_{III}}{K_I} \right|^{\frac{1}{\lambda_I - \lambda_{III}}} = \frac{r}{d_0^{13}} \left| \frac{1.0873\tau_T}{0.97786\sigma_0} \right|^{-8.184}. \tag{4.6}$$

Therefore, the dimensionless variables $\sigma_0/k$, $\tau_T$ needed to give a plastic radius $r_p/a$ are

$$\frac{r_p}{a} = 0.4196 \frac{r_p}{d_0^{13}} \left[ \frac{\sigma_0/k}{\tau_T/k} \right]^{8.184}. \tag{4.7}$$

It should be noted here that the exponents are very large. Small changes in the loading will produce large differences in the plastic radius. Similarly, the magnitude of loading, $G_0^{13}$, is given by Equation 2.2. In non dimensionalised terms

$$\frac{G_0^{13}}{k} = 1.4511 \left( \frac{\tau_T}{k} \right)^{3.7275} \left( \frac{k}{\sigma_0} \right)^{2.7275}. \tag{4.8}$$

First, as $d_0^{13}/a > 1$ the solution cannot have mode $III$ dominance, and, from Equation 4.6 this occurs when

$$\tau_T \leq 1.1119\sigma_0 \tag{4.9}$$

Considering Figure 3.3a, we can choose an error that is acceptable. For example, if we choose 10% we can get the corresponding values of $G_0^{13}/k$ by reading off the plot at 0.1. So $G_0^{13}/k < 0.2$ implies almost true mode $I$ and $G_0^{13}/k > 5.6$ implies almost true mode $III$. We can transform the parameters to the loads we are applying to determine the regions of the load space which show mode $I$ and mode $III$ dominance. This is shown in Figure 4.2.

Secondly, for modes $I$ and $III$ loading we know that the maximum plastic radius will always lie at

$\theta = \pi/2$. We need to make sure that the plastic radius is not so large as to feel the effects of the nearest boundary: this is defined as the small scale yielding (SSY) limit. Taking the stress values at this point we can apply the Von Mises yield condition, setting the value of $r_p/a$ we can find the stresses required to violate the limits of SSY.

We define SSY to be when the plastic radius, $r_p$ normalised by the characteristic length of the problem $a$ reaches 1%. When it crosses this value we can say that the boundary will begin to affect the solution and our analysis using an infinite plane is no longer valid.

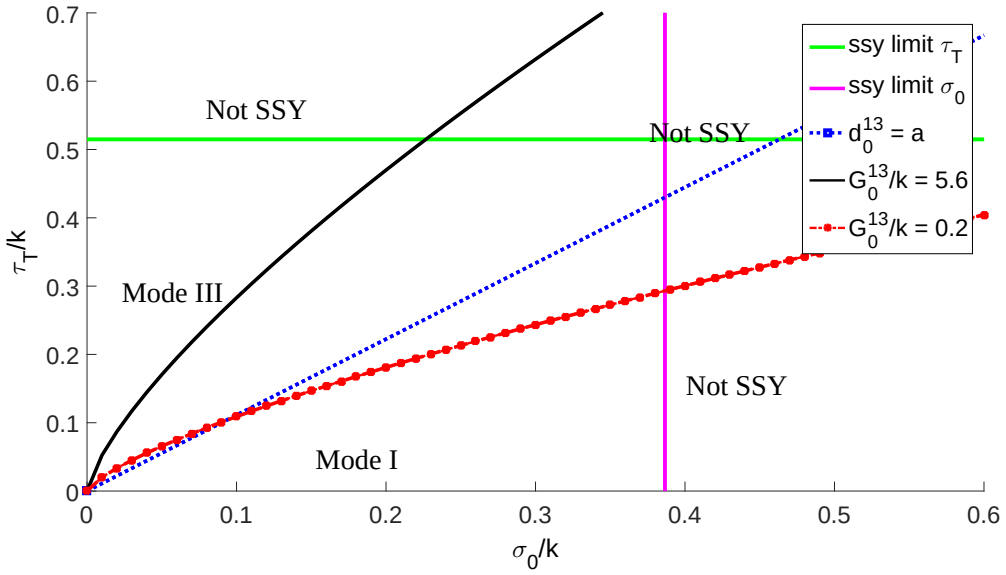
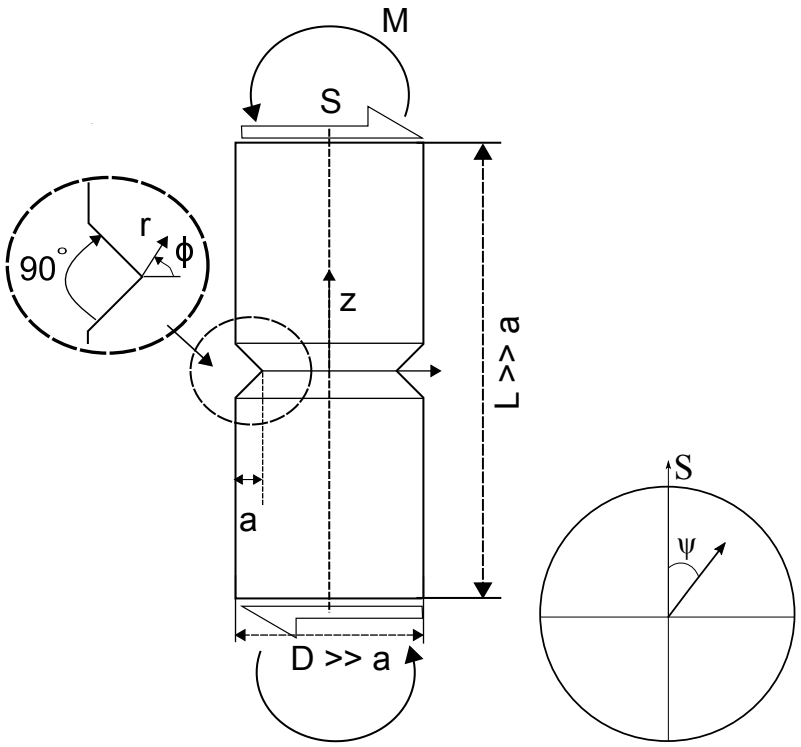



Figure 4.2: Dominance of modes along with SSY limits

## 4.2 Notched cylinder under shear (Mode $II$ and $III$)

To explore the mode $II$, $III$ loading combination we can retain the geometry, but apply a transverse shear force, as shown in Figure 4.3a. To maintain overall equilibrium, a bending moment gradient is present and we choose its value to be zero at the plane of the notch. The shear force will generate pure mode $II$ notch loading along the diameter in the direction of shear ($\psi = 0$) and pure mode $III$ along the diameter perpendicular to the shear direction ($\psi = \pi/2$). In all other locations we will see a mix of the two modes. The angle $\psi$ is defined on the plane and zero is defined to be in the direction of the shear load as shown in Figure 4.3b.

The calibrations for mode $II$, $III$ can be done in exactly the same way as mode $I$, $III$. This leads us to




(a) Mode $II$ and $III$ (b) Notch plane

Figure 4.3: Geometry of cylinder under shear

$$\begin{Bmatrix} K_{II}a^{\lambda_{II}-1} \\ K_{III}a^{\lambda_{III}-1} \end{Bmatrix} = \begin{bmatrix} 0.3875cos(\psi) \\ 1.4283sin(\psi) \end{bmatrix} \tau_0 \tag{4.10}$$

where

$$\tau_0 = \frac{S}{\pi(D/2)^2}. \tag{4.11}$$

From Equation 2.4, for this geometry we see that the magnitude of the loading, $G_0^{23}(\psi)$ varies around the notch in the form

$$\frac{G_0^{23}}{\tau_0} = 2.3393cos(\psi)(cot(\psi))^{0.3782} \tag{4.12}$$

We can choose values of $G_0^{23}/k$ so as to fix when the transition between modes $II$ and $III$ dominance occurs.

Considering the definition of $d_0^{23}$ we can eliminate a region of the graph which cannot have mode $II$ dominance ($d_0^{23}/a > 1$).

$$d_0^{23} = \left(\frac{1.4283\tau_0 sin(\psi)a^{\lambda_{III}-1}}{0.3875\tau_0 cos(\psi)a^{\lambda_{II}-1}}\right)^{\frac{1}{\lambda_{II}-\lambda_{III}}} \tag{4.13}$$

If we rearrange this equation then we are left with the inequality

$$\frac{d_0^{23}}{a} > 220.005(tan(\psi))^{4.1348} \tag{4.14}$$

to ensure that mode $II$ dominance cannot arise.

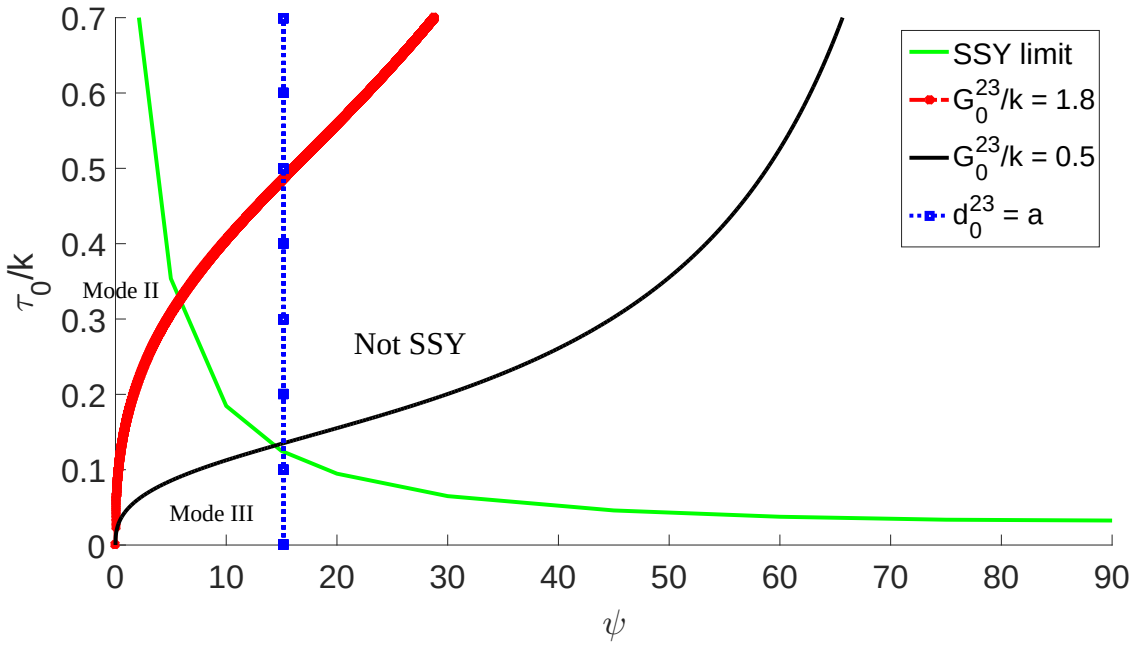



Figure 4.4: Dominance of modes with SSY limits

Figure 4.4 shows that at any non zero angle (given in degrees), measured on the horizontal plane from the direction of shear, light loads yield mode $III$ dominance. At very small angles, moderate levels of load yield mode $II$ dominance. The $d_0^{23} = a$ line signifies that beyond this angle, mode $II$ dominance is not possible. In this instance the loading and geometry will have violated SSY before this comes into effect.

# 5 Conclusion

It is shown that a new set of parameters $d_0^{ij}$, $G_0^{ij}$ are more informative than the three stress intensity factors when characterizing the state of stress near the root of a sharp notch. The $d_0^{ij}$ parameters tell us about the mode mixity. $d_0^{ij}$ also has units of length and serves as a partition between the two respective eigensolutions. The $G_0^{ij}$ parameters tell us about the magnitude of the loading. It has been shown under the most general loading that mode $I$ will dominate very close to the notch root and mode $II$ will dominate far away. The order of the $d_0^{ij}$ values also tells us if it is possible to have mode $III$ dominance. It should be noted that we have changed from three variables $(K_I, K_{II}, K_{III})$ to six variables. This implies that there are three equations which should connect the variables. Equation 2.5 is the first and most enlightening link between the six variables. A framework is established to apply

these results to a finite problem without further work and determine if they fall within the scope of small scale yielding. An extension to this work may be to consider the effect of elastic anisotropy and the presence of a notch tip radius.

# A Appendix

$$f_{rr}^{I}(\theta) = \frac{cos[(\lambda_I - 1)\alpha]cos[(\lambda_I + 1)\theta] - \frac{(\lambda_I - 3)}{(\lambda_I + 1)}cos[(\lambda_I + 1)\alpha]cos[(\lambda_I - 1)\theta]}{cos[(\lambda_I + 1)\alpha] - cos[(\lambda_I - 1)\alpha]} \tag{A.1}$$

$$f_{\theta\theta}^{I}(\theta) = \frac{cos[(\lambda_I - 1)\alpha]cos[(\lambda_I + 1)\theta] - cos[(\lambda_I + 1)\alpha]cos[(\lambda_I - 1)\theta]}{cos[(\lambda_I - 1)\alpha] - cos[(\lambda_I + 1)\alpha]} \tag{A.2}$$

$$f_{r\theta}^{I}(\theta) = \frac{sin[(\lambda_I - 1)\alpha]sin[(\lambda_I + 1)\theta] - sin[(\lambda_I + 1)\alpha]sin[(\lambda_I - 1)\theta]}{sin[(\lambda_I - 1)\alpha] - \frac{(\lambda_I + 1)}{(\lambda_I - 1)}sin[(\lambda_I + 1)\alpha]} \tag{A.3}$$

$$f_{rr}^{II}(\theta) = \frac{sin[(\lambda_{II} - 1)\alpha]sin[(\lambda_{II} + 1)\theta] - \frac{(\lambda_{II} - 3)}{(\lambda_{II} + 1)}sin[(\lambda_{II} + 1)\alpha]sin[(\lambda_{II} - 1)\theta]}{sin[(\lambda_{II} - 1)\alpha] - \frac{(\lambda_{II} - 1)}{(\lambda_{II} + 1)}sin[(\lambda_{II} + 1)\alpha]} \tag{A.4}$$

$$f_{\theta\theta}^{II}(\theta) = \frac{sin[(\lambda_{II} - 1)\alpha]sin[(\lambda_{II} + 1)\theta] - sin[(\lambda_{II} + 1)\alpha]sin[(\lambda_{II} - 1)\theta]}{-sin[(\lambda_{II} - 1)\alpha] + \frac{(\lambda_{II} - 1)}{(\lambda_{II} + 1)}sin[(\lambda_{II} + 1)\alpha]} \tag{A.5}$$

$$f_{r\theta}^{II}(\theta) = \frac{cos[(\lambda_{II} - 1)\alpha]cos[(\lambda_{II} + 1)\theta] - cos[(\lambda_{II} + 1)\alpha]cos[(\lambda_{II} - 1)\theta]}{cos[(\lambda_{II} - 1)\alpha] - cos[(\lambda_{II} + 1)\alpha]} \tag{A.6}$$

$$f_{rz}^{III} = -sin(\lambda_{III}\theta) \tag{A.7}$$

$$f_{z\theta}^{III} = cos(\lambda_{III}\theta) \tag{A.8}$$

# References


[1] M.L. Williams. Stress singularities resulting from various boundary conditions in angular corners of plates in extension. *J. Appl Mech.*, 19:526–528, 1952.

[2] M. Costabel and M. Dauge. General edge asymptotics of solutions of second order elliptic boundary value problems i, ii. *Proceedings of Royal Society of Edinburgh*, 123A:109155, 1993.

[3] M. Costabel, M. Dauge, and S. (Eds.) Nicaise. General edge asymptotics of solutions of second order elliptic boundary value problems i, ii. *Boundary Value Problems and Integral Equations in*

*Nonsmooth Domains. Lecture Notes in Pure and Applied Mathematics*, 167:Marcel Dekker, Inc., New York., 1994.

[4] M. Dauge. Elliptic boundary value problems in corner domains smoothness and asymptotics of solutions. *Lecture Notes in Mathematics*, 1341:Springer–Verlag, Berlin, 1988.

[5] V. G. Maz'ya, S. A. Nazarov, and B. A. Plamenvskii. Evaluation of the asymptotic form of the intensity coefficient on approaching corner or conical points. *U.S.S.R computational mathematics and mathematical physics*, 23:50–58, 1983.

[6] D. Leguillon and E. Sanchez-Palencia. Computation of singular solutions in elliptic problems and elasticity. *RMA 5 Masson, Paris*, 1987.

[7] P. Grisvard. Singularities in boundary value problems. *RMA 22, Masson, Paris*, 1992.

[8] P. Grisvard. Boundary value problems in non-smooth domains. *Pitman, London*, 1985.

[9] V. A. Kondrat'ev and O. A. Oleinik. Boundary-value problems for partial differential equations in non-smooth domains. *Russian Mathematics Surveys*, 38:1– 86, 1983.

[10] A. Carpinteri, P. Cornetti, N. Pugno, and A. Sapora. A finite fracture mechanics approach to structures with sharp v-notches. *Engineering Fracture Mechanics*, 75(7):1736–1752, 2008.

[11] A. Carpinteri, P. Cornetti, N. Pugno, and A. Sapora. Generalized fracture toughness for specimens with re-entrant corners: experiments vs. theoretical predictions. *Structural Engineering and Mechanics*, 32(5):609–620, 2009.

[12] A. Carpinteri, P. Cornetti, N. Pugno, and A. Sapora. On the most dangerous v-notch. *International Journal of Solids and Structures*, 47(7-8):887–893, 2010.

[13] S. Harding, A. Kotousov, P. Lazzarin, and F. Berto. Transverse singular effects in v-shaped notches stressed in mode ii. *International Journal of Fracture*, 164(1):1–14, 2010.

[14] G. B. Sinclair. Stress singularities in classical elasticity-i: removal, interpretation, and analysis. *Applied Mechanics reviews*, 57:251–297, 2004.

[15] G. B. Sinclair. Stress singularities in classical elasticity-ii: asymptotic identification. *Applied Mechanics reviews*, 57:385–439, 2004.

[16] A. Carpinteri, M. Paggi, and N. Pugno. Numerical evaluation of generalized stress-intensity factors in multi-layered composites. *International Journal of Solids and Structures*, 43(3-4):627–641, 2006.

[17] B. Atzori, P. Lazzarin, and G. Meneghetti. A unified treatment of the mode i fatigue limit of components containing notches or defects. *International Journal of Fracture*, 133(1):61–87, 2005.

[18] B. Atzori, P. Lazzarin, G. Meneghetti, and M. Ricotta. Fatigue design of complex welded structures. *International Journal of Fatigue*, 31(1):59–69, 2009.

[19] D. Leguillon. A criterion for crack nucleation at a notch in homogeneous materials. *Comptes Rendus De L'Academie Des Sciences Serie II Fascicule B-Mechanique*, 329(2):97–102, 2001.

[20] D. Leguillon. Strength or toughness? a criterion for crack onset at a notch. *European Journal of Mechanical a-Solids*, 21(1):61–72, 2002.

[21] P. Lazzarin and S. Filippi. A generalized stress intensity factor to be applied to round v-shaped notches. *International Journal of Solids and Structures*, 43(9):2461–2478, 2006.

[22] D.B. Bogy. Two edge-bonded elastic wedges of different materials and wedge angles under surface tractions. *ASME Journal of Applied Mechanics*, 38:377–386, 1971.

[23] D.B. Bogy and K.C. Wang. Stress singularities at interface corners in bonded dissimilar isotropic elastic materials. *International Journal of Solids and Structures*, 7:993–1005, 1971.

[24] C.C. Ma and B.L. Hour. Analysis of dissimilar anisotropic wedges subjected to antiplane shear deformation. *International Journal of Solids and Structures*, 25(11):1295–1309, 1989.

[25] C.C. Ma and B.L. Hour. Antiplane problems in composite anisotropic materials with an inclined crack terminating at a bimaterial interface. *International Journal of Solids and Structures*, 26 (12):1387–1400, 1990.

[26] P.E.W. Labossiere and M.L. Dunn. Calculation of stress intensities at interface corners in anisotropic media. *Engineering Fracture Mechanics*, 61(5-6):635–654, 1998.

[27] P.E.W. Labossiere and M.L. Dunn. Stress intensities at interface corners in anisotropic bimaterials. *Engineering Fracture Mechanics*, 62(6):555–575, 1999.

[28] M. Paggi and A. Carpinteri. On the stress singularities at multimaterial interfaces and related analogies with fluid dynamics and diffusion. *Applied Mechanics Reviews*, 61(2), 2008.

[29] D.A. Hills and D. Dini. Characteristics of the process zone at sharp notch roots. *Int. J. Solids and Struct.*, 48(14-15):2177–2183, 2011.

[30] R.C. Flicek, D.A. Hills, and D. Dini. Refinements in the characterisation of mode-mixity and small scale yielding at sharp notch roots. *Engineering Fracture Mechanics*, 126:73–86, 2014.

[31] D. Dini and D.A. Hills. Asymptotic characterisation of nearly-sharp notch root stress fields. *International Journal of Fracture*, 130(3):651–666, 2004.

[32] C. M. Churchman, D. Dini, and D. A. Hills. Closure at the root of a sharp notch. *International Journal of Mechanical Sciences*, 48(10):1063 – 1071, 2006.

[33] M. R. Ayatollahi, M. Dehghany, and M. Nejati. Fracture analysis of v-notched components - effects of first non-singular stress term. *International Journal of Solids and Structures*, 48(10): 1579 – 1589, 2011.